The Astrophysical Journal, 699:305–314, 2009 July 1 doi:10.1088/0004-637X/699/1/305

VARIABILITY TIMESCALES IN THE M87 JET: SIGNATURES OF E^2 LOSSES, DISCOVERY OF A QUASI PERIOD IN HST-1, AND THE SITE OF TeV FLARING

D. E. Harris[1], C. C. Cheung[2], Łukasz Stawarz[3,6], J. A. Biretta[4], and E. S. Perlman[5]
[1] Smithsonian Astrophysical Observatory, 60 Garden Street, Cambridge, MA 02138, USA; harris@cfa.harvard.edu
[2] NASA Goddard Space Flight Center, Astrophysics Science Division, Greenbelt, MD 20771, USA
[3] Kavli Institute for Particle Astrophysics and Cosmology, Stanford University, Stanford, CA 94305, USA
[4] Space Telescope Science Institute, 3700 San Martin Drive, Baltimore, MD 21218, USA
[5] Physics and Space Sciences Department, Florida Institute of Technology, 150 West University Boulevard, Melbourne, FL 32901, USA
Received 2008 November 13; accepted 2009 April 24; published 2009 June 11

ABSTRACT

We investigate the variability timescales in the jet of M87 with two goals. The first is to use the rise times and decay times in the radio, ultraviolet, and X-ray light curves of HST-1 to constrain the source size and the energy loss mechanisms affecting the relativistic electron distributions. HST-1 is the first jet knot clearly resolved from the nuclear emission by *Chandra* and is the site of the huge flare of 2005. We find clear evidence for a frequency-dependent decrease in the synchrotron flux being consistent with E^2 energy losses. Assuming that this behavior is predominantly caused by synchrotron cooling, we estimate a value of 0.6 mG for the average magnetic field strength of the HST-1 emission region, a value consistent with previous estimates of the equipartition field. In the process of analyzing the first derivative of the X-ray light curve of HST-1, we discovered a quasi-periodic oscillation which was most obvious in 2003 and 2004 prior to the major flare in 2005. The four cycles observed have a period of order six months. The second goal is to search for evidence of differences between the X-ray variability timescales of HST-1 and the unresolved nuclear region (diameter $<0\farcs6$). These features, separated by more than 60 pc, are the two chief contenders for the origin of the TeV variable emissions observed by H.E.S.S. in 2005 and by MAGIC and VERITAS in 2008. The X-ray variability of the nucleus appears to be at least twice as rapid as that of the HST-1 knot. However, the shortest nuclear variability timescale we can measure from the *Chandra* data ($\leqslant$20 days) is still significantly longer than the shortest TeV variability of M87 reported by the H.E.S.S. and MAGIC telescopes (1–2 days).

Key words: galaxies: active – galaxies: individual (M87) – galaxies: jets – radiation mechanisms: non-thermal – radio continuum: galaxies – X-rays: general

Online-only material: color figures

1. INTRODUCTION

We have been monitoring the jet of M87 in the X-rays with *Chandra* and the ultraviolet (UV, at $\lambda = 220$ nm) with the *Hubble Space Telescope* (*HST*) since 2002 January, and in the radio since 2003 (VLA, primarily at 15 GHz) and 2005 (VLBA, primarily at 1.7 GHz). Previous papers from this project include Paper I reporting our first results (Harris et al. 2003), Paper II which focused on the *HST* data (Perlman et al. 2003), Paper III which was mainly on the X-ray light curve of HST-1 which delineated the massive flare in 2005 (Harris et al. 2006) and Paper IV, the VLBA results showing superluminal proper motions in HST-1 (Cheung et al. 2007).

In this paper (V of the series), we present an analysis of the light curves for the nucleus, the jet knot HST-1 which is $0\farcs86$ from the core and which is the site of the massive X-ray, UV, and radio flare described in Paper III, knot D, and knot A. Knot A was mainly used as a control source since we do not expect short-timescale variability because it is well resolved in all bands. The light curve of knot D illuminates the effects of HST-1 on adjacent regions since it appears to have very little if any intrinsic variability on the timescales of interest here. In Sections 2–4, we describe the data and the analyses methods. In Section 5 we use the rising segments of the light curves to derive upper limits on the size of the emitting regions, and in Section 6 we examine the decay timescales of HST-1 in X-rays, UV, and radio bands in order to isolate signatures of E^2 losses. We describe newly discovered oscillations in the brightening and fading of HST-1 in Section 7. Finally, in Section 8, we discuss the evidence for short timescales in the X-ray variability of the nucleus and HST-1 which is relevant to the question of the location of the variable TeV emission reported by the H.E.S.S. Collaboration (Aharonian et al. 2006), MAGIC (Albert et al. 2008), and VERITAS (e.g., Acciari et al. 2008). Some preliminary results from this work were reported in Harris et al. (2008).

We take the distance to M87 to be 16 Mpc (Tonry 1991) so that $1''$ corresponds to 77 pc. Throughout this paper we assume that the radio to X-ray emission from all parts of the M87 jet comes from synchrotron emission, as argued in our previous papers (I and III). In particular, we assume that the X-ray nuclear emission is dominated by synchrotron emission from components of the inner (unresolved) jet rather than by thermal processes associated with the accretion disk around the central black hole.

2. THE *CHANDRA* X-RAY DATA

Since 2002, we have observed M87 with *Chandra* 6–7 times each observing season with 5 ks exposures typically separated by 6 weeks. Additionally in 2005, near the maximum of the X-ray light curve of HST-1, we scheduled weekly observations to constrain shorter timescale variability (epochs Ya to Yg; see Table B1). After the report of variable TeV emission in the 2005 H.E.S.S. observations of M87 by Aharonian et al. (2006), we

[6] Also at Astronomical Observatory, Jagiellonian University, ul. Orla 171, 30-244 Kraków, Poland.

obtained Director's Discretionary Time (DDT) observations to sample the X-ray light curves on ∼2–3 day timescales during two "dark time" fortnights in February and March of 2007 when TeV observations were scheduled (epochs Ys to Zb). A total of 61 observations have been obtained from these programs thus far.

For details of our reduction procedures, see Papers I and III. Briefly, we use a 1/8th segment of the back illuminated S3 chip of the ACIS detector aboard *Chandra*. This permits us to have a frame time of 0.4 s with 90% efficiency. Although this setup was essentially free of pileup when Wilson & Yang (2002) tested various options during 2000 July, with the advent of the ever increasing brightness of HST-1, pileup (Davis 2001) became a major problem so we switched to a detector-based measure of intensity: keV s^{-1}. This approach uses the event 1 file with no grade filtering (so as to recover all events affected by "grade migration") and we integrated the energy from 0.2 to 17 keV so as to recover all the energy of the piled events. Other uncertainties for piled events come from the onboard filtering, the "eat-thy-neighbor" effect, and second-order effects such as release of trapped charge (see Appendix A).

2.1. Photometry

Although we used small circular apertures for fluxmap photometry in Paper I, the basic analysis for this paper adopts the rectangular regions used in Paper III so as to encompass more of the point-spread function (PSF). The four regions of interest (the core, HST-1, knots D and A) are shown in Figure 1; we did not use background subtraction because the photometric apertures were small.

All events within each rectangle are weighted by their energy and the sum of these energies, when divided by the exposure times, gives the final keV s^{-1} value used in the light curve. Uncertainties are strictly statistical, based on the number of counts measured: $\sqrt{N}/N$ and typically range from 1% to 5%.

To analyze and compare timescales, we measure the slope between adjacent measurements (and also between every other observation) by calculating the ratio, $(I_2 - I_1)/\Delta t$, where I_1 and I_2 are the intensities at the times t_1 and t_2 and $\Delta t(\mathrm{yr}) = t_2 - t_1$. To convert this to a fractional change we divide by $\min(I_1, I_2)$, so the definition of fractional change per year (fpy) is

$$\mathrm{fpy} = \frac{D}{I_i \Delta t}, \tag{1}$$

where $D = (I_2 - I_1)$. When the intensity is *increasing* ($I_1 < I_2$), the fpy has $i = 1$ and is denoted (when required), as fpy^+. When the intensity is *dropping* ($I_1 > I_2$), $i = 2$ and we specify by using fpy^-.

(Hereafter, the superscripts are suppressed where the signs are implicit). According to this definition, the doubling time for a given value of fpy is simply $t_{\mathrm{double}}(\mathrm{yr}) = 1/\mathrm{fpy}$, thus when $\mathrm{fpy} = \pm 1$, there was a rate of change which would produce a factor of 2 increase or decrease in I in one year.

The uncertainties in each value of I are propagated to the first derivative by calculating the square root of the sum of the squares of the errors on intensity. Denoting σ_i as the uncertainty of I_i, we express the error of fpy as

$$\sigma(\mathrm{fpy}) = \frac{1}{\Delta t} \times \frac{I_j}{I_i} \times \sqrt{\left(\frac{\sigma_1}{I_1}\right)^2 + \left(\frac{\sigma_2}{I_2}\right)^2}. \tag{2}$$

Here, $i = 1$, $j = 2$ for the error on fpy^+, and $i = 2$, $j = 1$ for fpy^-.

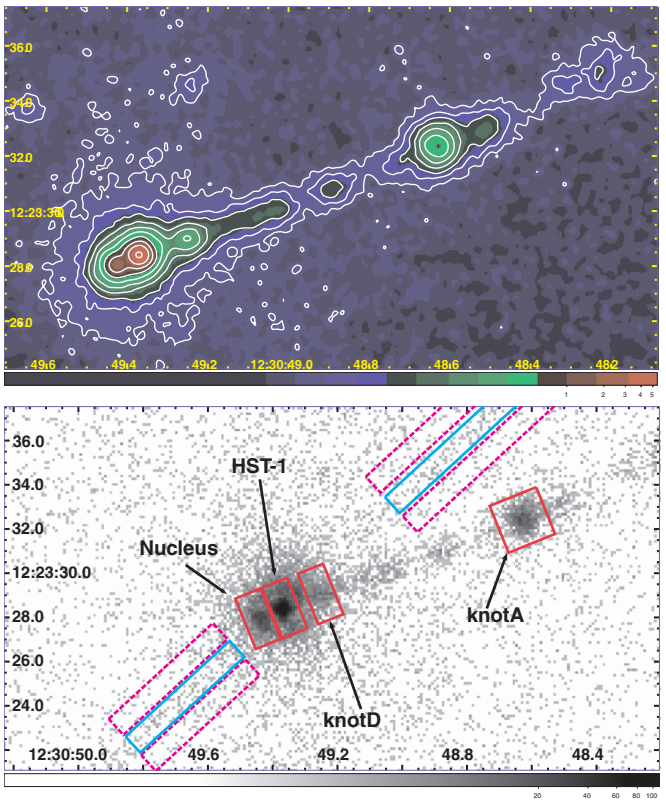

Figure 1. *Chandra* X-ray image constructed from the sum of our data from 2002 to 2004. This is a total power image for which each event has been multiplied by its energy. In the top panel, a Gaussian smoothing function of FWHM = 0.″25 has been applied. Contours start at 0.01 eV s^{-1} per 0.″049 pixel and increase by factors of 2. The second panel shows the regions used for photometry. The four rectangular regions in red (from left to right) are the nucleus, the flaring knot HST-1 (0.″86 from the nucleus), knot D, and knot A. The long thin cyan rectangles and the dotted magenta rectangles are used for "readout streak photometry" ("on" and "background," respectively)—see Section 2.2. The image is a 5 ks exposure from 2005 May when HST-1 was close to its peak intensity. Pixel randomization has been removed and in this figure panel, the events are binned into 0.″123 pixels. The axes are J2000 coordinates.

The fpy values are plotted in Figure 2 for the nucleus, HST-1, knots D and A. The latter two features serve as controls, and display the expected behavior for a steady source: at long-time intervals, fpy values are consistent with zero and have small uncertainties. The errors increase as Δt decreases. Since all errors are 1σ ($\sqrt{N}/N$), some values for knots D and A appear to be different from zero, as expected.

In the next section, we discuss using the readout streak for estimating source intensity and in the Appendix (Appendix A) we describe some of the other problems engendered by pileup.

2.2. Photometry of the Readout Streak

The only check we have been able to devise is "readout streak photometry" (see also Marshall et al. 2005). For this procedure, we isolate the segments of the readout streak which are not close to the jet. With long thin rectangles ($n \times 2$ pixels; Figure 1), and adjacent rectangles to measure the background, we estimate the effective exposure time for the net counts as (number of frames) $\times n \times 41$ μs, where n is the length of rectangles in pixels. In a typical 5 ks observation, we are thus able to get the equivalent of 30–40 s worth of continuous clocking mode data which are free of pileup effects but suffer from poor signal-to-noise ratio (S/N) because of the necessarily large background area. While

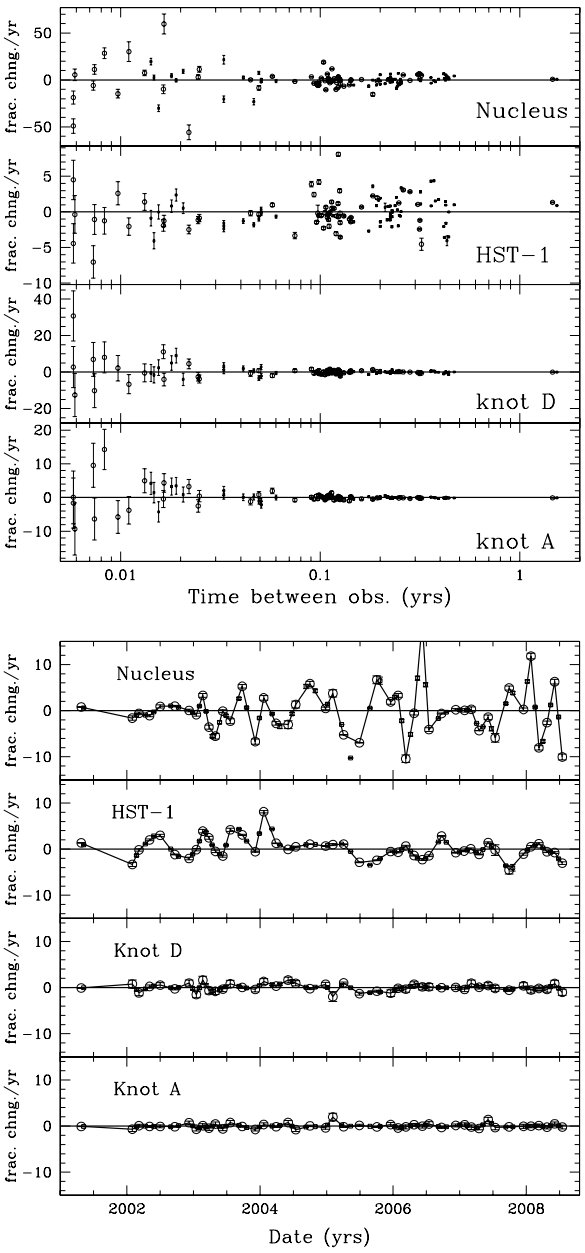

Figure 2. First derivative of the light curves for the nucleus, HST-1, knots D and A (top to bottom). The smaller squares are values from intensity pairs which skip the intervening observation and are thus not independent of the larger circles (adjacent observations). In the upper panel the x axis is the time between observations; in the lower panel it is the date. The y axis is fpy. Note the change in y scale for different plots in the upper panel, but in the lower panel we have set the max/min values to ± 15. In the lower panel, intervals with closely spaced observations have been averaged to avoid large error bars arising from small Δt.

the general behavior of the streak photometry is consistent with the expectation that it would become increasingly larger than the standard photometry as the intensity of HST-1 increased (more pileup and more onboard rejection), there are a few unexpected departures from this behavior. In particular, there are some high values where both methods give the same intensity, and there is one segment of low intensity where the streak photometry is significantly less than the standard photometry. For these reasons, we rely on our "standard" photometry and relegate the results of the readout streak photometry to the status of "caveats" and "alternate possibilities."

3. THE UV DATA

The UV data used in this paper were obtained from a series of *HST* proposals (Biretta, PI) which were synchronized with the *Chandra* observations although for various reasons not every *Chandra* observations has a corresponding *HST* observation. The data were reduced with the usual procedures and will be described in a separate paper (J. A. Biretta 2010, in preparation).

4. THE RADIO DATA

The VLA[7] 15 GHz observations were obtained as part of our multifrequency program coordinated with the *Chandra* and *HST* monitoring and began mid-2003. In each VLA cycle, we observed M87 in three 8 hr runs (program codes AH822, AH862, AH885, AC843): two in A array followed by one in B array. The beam sizes were typically around 0.″15 and 0.″4, respectively. The longer gaps occur during C and D array configurations when the angular resolution is not sufficient to separate the nucleus and HST-1.

The observations utilized two adjacent 50 MHz wide intermediate frequencies centered at 14.94 GHz. A total of 1–1.5 hr of on-source time was split between 9 and 10 scans over each 8 hr run to obtain good (u, v) coverage. The data were calibrated in AIPS (Bridle & Greisen 1994) with the flux density scale set using scans of 3C286 and the initial phase corrections determined with a nearby calibrator. Subsequent phase and amplitude self-calibration was performed using the Caltech DIFMAP package (Shepherd et al. 1994).

An additional archival B-array data set (BK073) was analyzed to give us the data point in 2000 January, before our monitoring began. The observation used an identical setup to ours but with only four 3.5 min scans obtained. This was sufficient to detect a faint (2.8 mJy) feature at the position of HST-1, thus providing a baseline measurement to our subsequent ones.

5. ESTIMATING THE SIZE OF EMITTING VOLUMES FROM RISE TIMES

As described in earlier papers of this series, the rise of the light curve can give estimates of the source size so long as the beaming parameters—the bulk Lorentz factor of the jet (Γ), the angle between the jet and our line of sight (θ), and the Doppler beaming factor (δ)—are not changing.

For the standard analysis of the X-ray light curve of HST-1, the largest observed slope occurred early in 2004 and had a value of fpy $= 8$ (Figure 2); the intensity doubled during our 6 week sampling interval. Thus, we are able to set an upper limit to the characteristic size of the emitting region in the jet frame of diameter $\leqslant 0.12\delta$ light years (45 light days). Significantly, larger values of fpy occur for the HST-1 light curve generated from the readout streak photometry (Section 2.2), but these have large uncertainties so do not yield useful limits on the source size.

The smallest directly measured value for the size of HST-1 comes from the VLBA beam size of 3 mas which corresponds to 0.7 light years (Paper IV). If the X-ray and radio-emitting volumes were to be one and the same (i.e., the upstream end of HST-1), and if the radio size is actually similar to our VLBA resolution, then δ would be of order 5, a value similar to that estimated in our previous papers.

[7] The VLA is operated by the National Radio Astronomy Observatory, which is a facility of the National Science Foundation, operated under cooperative agreement by Associated Universities, Inc.

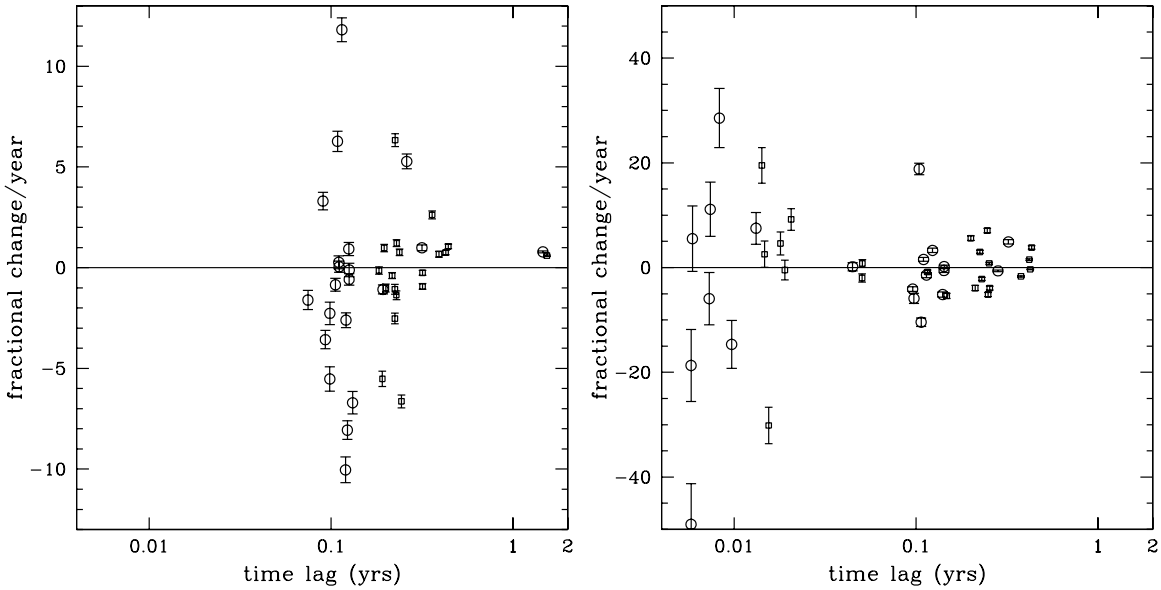

Figure 3. Fpy values for the nucleus. The larger open circles come from adjacent observations while the smaller squares are data pairs formed by skipping the adjacent observation. First panel: the period from 2000 to 2004 and 2008 when the HST-I intensity was low (<2 keV s^{-1}). Second panel: the period 2006–2007 when the intensity of HST-1 was between 2 and 4 keV s^{-1}.

Because of the second-order effects which were prevalent when HST-1 was strong, we have restricted our analyses of the nuclear fpy data to (a) 2000–2003 plus 2008 when HST-1 was at a low intensity (less than 2 keV s^{-1}), and (b) 2006–2007 when the HST-1 intensity was at an intermediate value (2–4 keV s^{-1}). The data between 2 and 4 keV s^{-1} are used because this time interval includes the closely spaced observations of 2007. We believe the second-order effects for this intensity regime are minimal because although the light curve of the nucleus shows a very obvious feature corresponding to the peak of HST-1 in 2005, there is no apparent correlation between the intensity of the nucleus and that of HST-1 for the 2006–2007 data. These data are shown in Figure 3.

During low-intensity intervals, the maximum value of fpy^{+} was about 12 (a light travel time of 30δ light days), although there were no closely spaced observations during these periods so that larger fpy^{+} values may have been missed because of inadequate sampling. When HST-1 was at intermediate levels (~2–4 keV s^{-1}), we had the closely spaced observations during 2007 February and March from the DDT project and the maximum fpy^{+} for the core was 28.5 ± 5.6, but we take a value of 19 (light travel time: 19δ light days) as a characteristic value since the second largest value was 18.8 ± 1.1.

6. ANALYSIS OF THE DECAY PHASES OF THE LIGHT CURVES OF HST-1

In this section, we analyze the decay of the light curves of HST-1 at X-ray, UV, and radio wavelengths (Figure 4). We will not attempt to make a parallel investigation of the nuclear emission because we have no information as to the size of the emitting volume or its geometry, the interpretation of the UV data would be problematic, and although likely, it remains to be demonstrated that the nuclear X-ray emission is actually nonthermal emission from the inner jet rather than from some thermal process associated with the accretion disk or its environs.

The decay of the light curve may be caused by several effects but has the potential to reveal which processes are dominant. If all bands have similar rates of decreasing intensity, the most likely cause is either a change in the beaming factor (as might arise from a change in θ) or a general expansion which reduces the energy of all electrons according to their energy (the so-called E^1 losses) as well as reducing the magnetic field strength. Note however that if the emitted spectrum is not a simple power law, but for example steepens at high frequencies, then a simple expansion may produce a much stronger decay at high frequencies both because the previously "viewed" electrons for a fixed observing band are now replaced by the fewer (previously higher energy) electrons and also because of the weaker B field, the fixed observing band now comes from an even higher energy segment of the electron distribution.

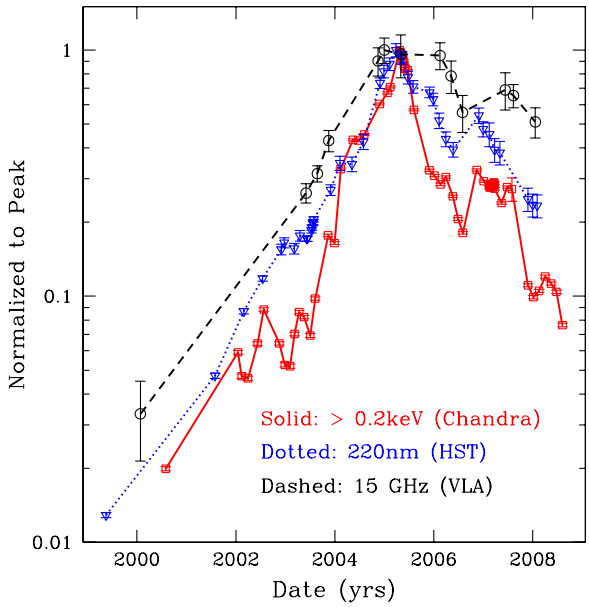

Figure 4. X-ray, UV, and radio light curves of HST-1. The intensity is plotted on a log scale to demonstrate the overall conformity between bands. Each curve has been normalized by setting the peak value to unity so as to permit visual comparison of the decay. The peak values are 12.417 keV s^{-1} (X-ray); 0.596 mJy (UV); and 0.084 Jy (15 GHz).

(A color version of this figure is available in the online journal.)

Our preliminary analysis of Paper III indicated that the initial decrease of the major flare had a similar timescale as the preceding rise, and that this might be indicative of either a changing δ, or a compression and subsequent expansion. However, it has become clear that although the UV and X-ray light curves appeared to have a similar behavior initially, there are instrumental effects present which were not recognized, there are significant differences in the UV and X-ray decays and the radio intensity did not conform to the rapid decay seen at higher frequencies (Figure 4).

We investigate two aspects of this problem. First, we examine the behavior of the UV and radio light curves at times when large rates of decay are observed at X-rays and second, we compare the fpy values between bands without regard to when they occurred. Both of these approaches suffer from the sparser sampling in the radio. Although most of the UV data were obtained within a week of the *Chandra* observations, not every *Chandra* observation has a corresponding *HST* observation.

6.1. Comparison of Particular Time Segments

This approach is based on the assumption that all three wavelength bands come from the same emitting volume. If however, the emitting volume is "layered" (e.g., concentric spheres with longer wavelengths coming from larger volumes), then it would be possible to have different characteristic decay times for each layer (assuming different values of the magnetic field strength), and the decays in the light curves would not have to happen at the same time since the cessation of injection of particles and fields would not necessarily be simultaneous in all emitting volumes.

The most significant (i.e., without excessively large uncertainties) decays in the X-ray light curve occurred in (a) 2002.0 (fpy $= -3.32 \pm 0.45$), (b) 2005.5 (fpy $= -3.51 \pm 0.08$), and (c) 2007.7 (fpy $= -4.53 \pm 0.85$).

For event (a), we have no relevant radio values of fpy and the UV sampling was not sufficient: the UV intensity rose from 28 to 52 μJy between 2001.58 and 2002.16. The decay in the X-rays occurred between 2002.044 and 2002.119.

Event (b) occurred after the peak of the giant flare. This is perhaps the best example of what might be expected from E^2 losses affecting the electron energy distribution (see Figure 4). However, as mentioned above, we cannot rule out the possibility of an expansion of the source if the X-rays are coming from a segment of the electron distribution that is falling more rapidly than the power law connecting the UV to the X-ray. The fpy value for the UV is -0.85 ± 0.86.

The third notable decline in the X-ray light curve came during the three months in 2007 while M87 was behind the Sun (August to November). Unfortunately, the UV monitoring had a much longer gap (almost seven months) so the relevant data for a direct comparison do not exist.

If the X-ray fpy$^-$ value of -3.5 during the main decay phase ("event b," Figure 5) was dominated by E^2 losses, we can make an order of magnitude estimate for the magnetic field strength. Note that we do not consider here a detailed evolution of the synchrotron flux produced by the radiatively cooling electron energy distribution as considered in, e.g., Kardashev (1962), but we can approximate the cooling time required to drop the intensity by a factor of 2 by assuming that this decay is caused by a factor of 2 fewer electrons with energies providing the bulk of the observed X-rays between 0.2 and 6 keV. Further, we assume the exponent of the electron distribution, $p = 2\alpha_x + 1 = 3.4$, which is our best estimate for the spectrum of HST-1 in the X-ray band (Harris et al. 2006). Since dE/dt to first approximation

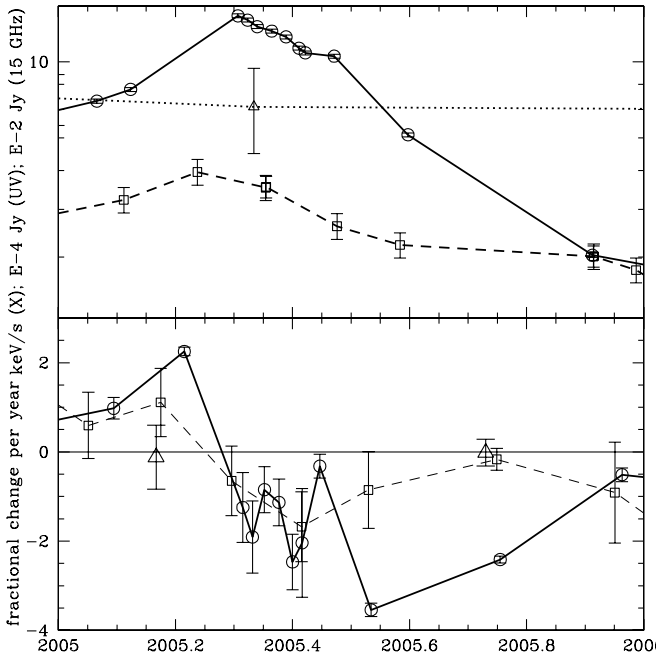

Figure 5. Multiband data for HST-1 during 2005. The top panel shows the light curves: circles for X-ray; squares for UV with the dashed line; and triangles for the 15 GHz data (dotted line). The lower panel shows the corresponding fpy values, the first derivative of the light curves. Coding is the same as the upper panel except no line is added to the two radio data, both of which are consistent with zero. Note that the shoulder in the UV light curve following the peak. This can also be seen in Figure 4, and leads to the much smaller values of dI/dt for the UV than for the X-ray. The radio light curve is essentially "flat topped" and shows no change during the year.

shifts the power-law distribution, $N(E)$ to lower energies, we require an energy shift of $2^{-1/3.4}$ or 0.8. We then ask what magnetic field strength, B is required to produce a 20% energy loss in the time, τ, it takes for the intensity to fall by a factor of 2. The observed time, τ_o is $1/3.5 = 0.28$ yr; in the jet frame $\tau' = \delta\tau_o$ where δ is the beaming factor.

With the standard Equations (3.28) and (3.32) from Pacholczyk (1970), setting $\tau' dE/dt = 0.2E$ (where E is the energy of the electron), and changing jet frame parameters to the observer frame, we find

$$B \approx 0.5\delta^{-1/3} \left(\frac{\tau_o}{\mathrm{yr}}\right)^{-2/3} \left(\frac{\varepsilon}{\mathrm{keV}}\right)^{-1/3} \mathrm{mG}\,. \qquad (3)$$

Here, $\tau_o/\mathrm{yr} \equiv 1/\mathrm{fpy}^-$ is the observed time for the intensity to drop by a factor of 2 and ε is the characteristic energy of the X-ray band. For our parameters, this reduces to $B\delta^{1/3} = 1.1$ mG, and for $\delta = 5$, 0.6 mG, a value reasonably consistent with the 1 mG derived on the basis of equipartition conditions for HST-1 before the major flare (Paper I).

If E^2 losses were the controlling factor in the light-curve decay, we would expect τ(UV) to be longer by the square root of the ratio of the frequencies, $\approx$14. The actual observed τ(UV) is $1/0.85 = 1.18$ yr although the uncertainties include much longer times (fpy $= 0$ is within the 1σ error). Of course the fact that both the UV and the radio intensities decline significantly at later times indicates that expansion of the source is probably a major contributor to the light-curves behavior during some intervals.

6.2. Comparison of Extreme Values of dI/dt

In Figure 6, we plot the fpy values for HST-1 in different bands. Although many of the uncertainties are large, and the

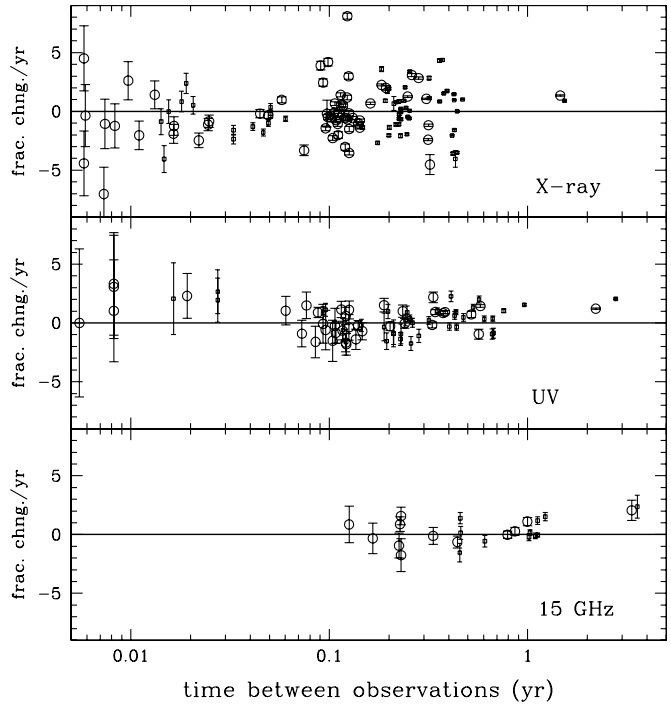

Figure 6. X-ray, UV, and radio scatter plots of fpy values for HST-1. The smaller square points are for every other observation and are thus not independent of the data for adjacent observations (larger circles). Top to bottom: X-ray, UV, and 15 GHz. The absence of large values at large times in the top panel arises from the smaller intervals between observations: if we had calculated fpy for every possible pair of observations, we would have recovered the data describing the giant flare.

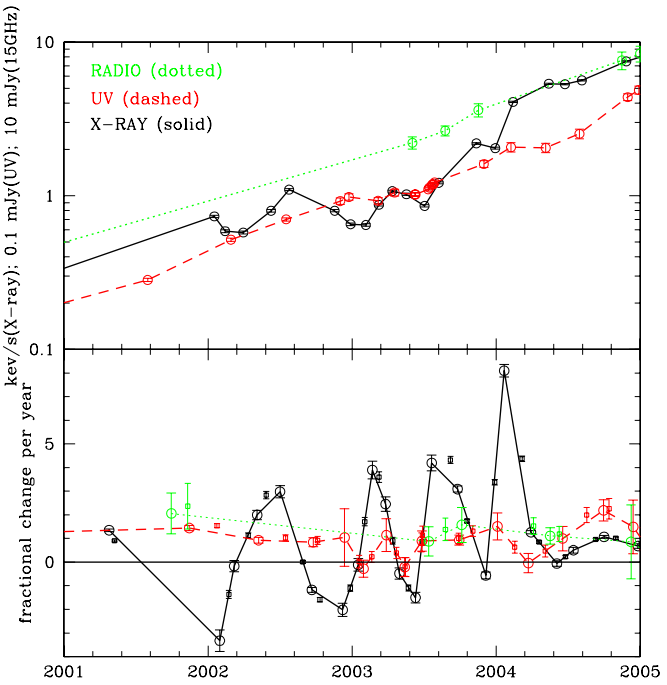

Figure 7. Upper panel: light curves of HST-1: X-ray (solid), UV (dashed), and radio (dotted). Lower panel: fpy values for HST-1 prior to the giant flare. Larger circles are the primary data from adjacent observations. Smaller circles are generated from every other observation. The curves connect primary data.

(A color version of this figure is available in the online journal.)

sampling in the radio is clearly insufficient, we find that the largest (absolute value) believable negative fpy's are −5, −2, and −1 for the X-ray, UV, and radio, respectively. We take this as evidence that energy loss by expansion alone is not indicated. The obvious caveat to this conclusion is that there is a spectral break in the optical/UV in the sense that $\alpha_{ox} > \alpha_{ro}$. If there is additionally a curving downward of the spectrum in the $\nu = 10^{16}$–10^{18} Hz band, we could explain the fpy data with just expansion.

7. DISCOVERY OF IMPULSIVE BRIGHTENING IN HST-1 VIA dI/dt

Close examination of Figures 2 and 7 (upper panel) shows that the X-ray light curve has a series of small peaks superposed on a gradually rising intensity between 2002 and 2004. Their reality is demonstrated by the plot of the first derivative (Figures 2 and 7). Characteristic times of this oscillation (peak-to-peak or trough-to-trough) range from 0.50 yr (most common) to a maximum value of 0.84 yr. Although there are some slightly discernible features on the fpy(UV) plots, the data are not sufficiently numerous or robust enough to search for lags between bands. The impulses are not evident at radio frequencies and their existence is debatable for the UV although if they were as large in the UV as in the X-ray, they should have been detected.

Although the causes of these oscillations are not known, we speculate that a quasi-periodic variation in the conversion of bulk kinetic jet power to the internal energy of the radiating plasma is more likely than a modulation of power flowing down the jet. We also disfavor a changing beaming factor caused by a changing angle to the line of sight (e.g., a "thrashing jet"). For jet modulation, a thrashing jet, and periodic compression and expansion, we would expect any oscillation to be evident at all frequencies equally. The absence of oscillations in the UV encourages us to look for an oscillating injection of particles which, for the highest energy electrons is made manifest by the short lifetimes, but for the electrons radiating at lower frequencies, gets smoothed out by the continuously accumulating total number of radiating particles.

8. COMPARING X-RAY TIMESCALES OF HST-1 AND THE NUCLEUS TO EVALUATE THE SITE OF TEV FLARING

To date, there have been two reports of TeV short-timescale flaring from M87: 2005 April (H.E.S.S., Aharonian et al. 2006) and 2008 February (MAGIC, Albert et al. 2008); (VERITAS, e.g., Ergin 2008). While the angular resolution of the TeV systems does not permit a location to be determined, the expected relation between X-ray intensity and TeV intensity via an inverse Compton model holds the potential of localizing the site of the TeV emission if an unambiguous feature in the TeV light curve can be associated with one in the X-rays. Moreover, since both instances of TeV flaring appeared to be characterized by timescales of only a few days, it is also possible to evaluate statistical differences in X-ray timescales, particularly for the two leading contenders, the nucleus and HST-1.

There are a few striking differences in Figure 2 between the nucleus and HST-1. For the nucleus, there are quite large values of fpy at short timescales, whereas HST-1 has an order of magnitude smaller amplitudes and these occur at somewhat longer timescales. We interpret the presence of large amplitudes at short sampling times together with smaller amplitudes at longer times to mean that we can characterize the nuclear variability as a sort of "flickering." HST-1 of course provided us

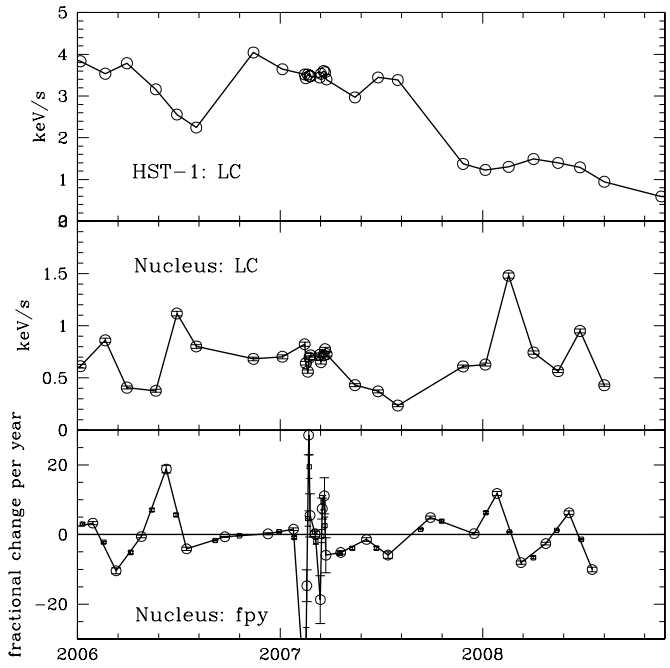

Figure 8. First derivative of the nucleus from 2006 during which time HST-1 was <4 keV s^{-1}. The top panel is a segment of the light curve of HST-1 and the middle panel shows the light curve for the nucleus with 5% of HST-1 subtracted. There are no egregious signatures of contamination. The bottom panel shows the first derivative of the nuclear light curve with smaller squares for intensity pairs with an intervening observation.

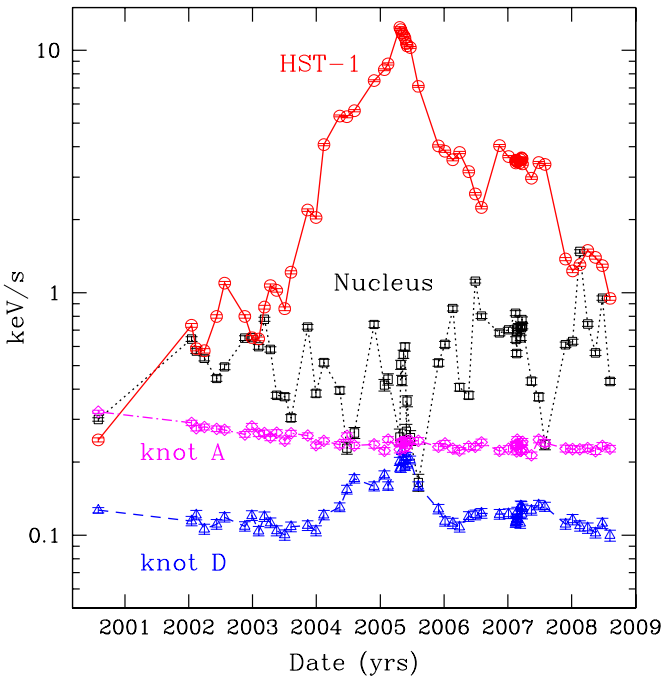

Figure 9. X-ray light curves for the nucleus (squares), HST-1 (circles), knots D (triangles) and A (diamonds). 5% of the intensity of HST-1 has been subtracted from the nuclear values. We consider it highly probable that most/all of the knot D apparent variability is simply contamination from HST-1, and the slight shift to later time of the peak in 2005 is caused by the secondary response (release of trapped charge) of the HST-1 PSF. The secular decline of the knot A light curve is roughly consistent with the loss of effective area at low energies caused by contamination buildup on the ACIS filter.

(A color version of this figure is available in the online journal.)

with a major flare with a timescale of a year or more (Figures 4 and 9). The energy emitted by the nuclear flickering is a small fraction of the energy emitted by the flaring of HST-1, but the timescales are quite different.

In Paper IV, we argued that the site of the TeV flaring observed by H.E.S.S. could be HST-1, whereas others (e.g., Georganopoulos et al. 2005, Tavecchio & Ghisellini 2008, and see also Levinson 2000) have suggested a location closer to the supermassive black hole (SMBH). We pointed out that besides the coincidence of the peak of the HST-1 (X-ray, UV, radio) light curve occurring at the same time as the H.E.S.S. event in 2005, we knew that HST-1 was physically small (from the VLBA observations and from the X-ray variability), that the emitted power at TeV energies was comparable to the X-ray power (linked, for example, by a synchrotron self-Compton (SSC) model), and that there were difficulties of getting TeV photons out from the immediate vicinity of the SMBH. While none of these considerations have changed, our current analyses on timescales could be thought of as circumstantial evidence that the nuclear X-ray emission comes from a smaller emitting volume than that of HST-1 and that this smaller emission region could be the same as that producing the TeV flares, even though our upper limits on the size of the X-ray-emitting region are still much larger than the light day timescales inferred for the TeV region.

Early in 2008 February, we detected an increase in the nuclear X-ray emission to a level a bit higher than it has ever been (Figures 8 and 9). This single *Chandra* observation was made during the TeV flaring observed by MAGIC and VERITAS and the corresponding values of fpy were $\mathrm{fpy}^{+} = +11.8 \pm 0.6$ and $\mathrm{fpy}^{-} = -8.0 \pm 0.5$. So far in 2008, HST-1 has been at a low level with only small changes in amplitude. Unfortunately, we do not have a good estimate of X-ray timescales for the 2005 H.E.S.S. event. Although we had a series of weekly observations, the large fpy(nuclear) values could have been contaminated by rapid changes in HST-1, as indicated by fpy(HST-1) measurements derived from the readout streak photometry. If there is substantial TeV flaring in 2009, we may be able to settle this question via an approved target of opportunity *Chandra* proposal which aims to find correlated X-ray/TeV behavior in the respective light curves.

9. SUMMARY

We have found a quasi-periodic impulsive signature in the brightening and dimming of HST-1 in the X-rays. While this could be interpreted as a manifestation of past modulation of jet power, we suspect that it is rather a local oscillation of the process that converts bulk kinetic jet power to the internal energy of the emitting plasma. The fact that HST-1 lies on the northern edge of the cone defined by the VLBA jet (Paper IV) and that the cross section of HST-1 is less than 0.1% of the jet area (the cone of the VLBA jet has a diameter of ≈90 mas at the distance of HST-1 whereas the effective diameter of the unresolved upstream end of HST-1 is ≈2.5 mas), leads us to speculate that the time varying acceleration of electrons is related to a local instability. The ratio of <0.1% in areas is consistent with the ratio of power emitted by HST-1 to that believed to be the kinetic power of the jet (Bicknell & Begelman 1996).

The finding that the decay times of the light curves of HST-1 progressively lengthen moving from high to low frequencies suggests that simple expansion is not the primary energy loss mechanism for the relativistic electrons. If the X-ray decay time actually reflects the synchrotron half-life of the highest energy electrons, we are not only able to estimate a value of the

magnetic field which is independent of the usual equipartition assumptions, but also to provide an explanation of why the impulsive brightening is seen only at X-rays. That is because the period of the oscillations is very similar to the X-ray decay time. The UV decay time is of order 10 times longer, so that an oscillating brightening would be smoothed out by the failure of the UV radiating electrons to lose their energy before the next brightening. The similarity of the decay time to the oscillatory brightening (both at X-ray frequencies) may be a coincidence (which makes the effect manifest), or it could be a causal component of the (as yet to be determined) instability mechanism.

The X-ray variability timescale evidence suggests that the nucleus displays faster variability than does HST-1. This is circumstantial evidence for the hypothesis that the site of the flaring TeV emissions is the unresolved nucleus rather than HST-1. However, the shortest nuclear variability timescale we can measure from the *Chandra* data ($\leqslant$20 days) is still significantly longer than the shortest TeV variability of M87 reported by the H.E.S.S. and MAGIC telescopes (1–2 days).

The analogy we find useful in thinking about HST-1 is that of a river representing the underlying power flow of the jet. When something occurs to transfer some fraction of this power flow into a radiating plasma, we think of this as "white water." While knot A might be compared with a waterfall, HST-1 is more like a rock in the river. Thus, the giant flare could have been caused by a change in local conditions (e.g., something moving into the river), with the resulting bits of white water carried downstream as the observed radio blobs.

We acknowledge the *Chandra* Director's Office for approving our request to obtain a series of observations with short intervals in 2007 February and March. Those data were of critical importance in distinguishing timescale differences between the nucleus and HST-1. A. S. Wilson (deceased) and W. Sparks were co-investigators on the yearly *Chandra* proposals. We have benefited from discussions with R. Blandford; with colleagues in the "TeV community," particularly H. Krawczynski, P. Collin, and M. Hui; with F. Primini on aspects of error propagation; and with B. Wargelin, G. Allen, and R. Edgar for advice on the subtle aspects of the ACIS CCD. We thank the anonymous referee for a useful critique.

Work at SAO was supported by NASA grants GO6-7112X, GO7-8119X, and GO8-9116X. C.C.C. acknowledges support from NRAO through a Jansky Postdoctoral Fellowship (2004–2007) and the NASA Postdoctoral Program at Goddard Space Flight Center, administered by Oak Ridge Associated Universities through a contract with NASA. Ł.S. acknowledges support by MEiN through the research project 1-P03D-003-29 in years 2005–2008. E.S.P. acknowledges support from the NASA LTSA program through grant NNX07AM17G.

Facilities: VLA, *HST*, *CXO* (ACIS)

APPENDIX A

PILEUP PROBLEMS

A.1. Saturation

Although the methods of Section 2 recover most of the intensity of piled sources, there are onboard filters that keep events with energies >17 keV or with certain bad grades from being telemetered to the ground. We suspect that these filters produced a significant decrease in our measurements when HST-1 was near its peak intensity, but we have not been able to verify this directly since the housekeeping files that provide the number of events "dropped" because of amplitude and grade appear to be dominated by cosmic-ray events.

A.2. "Eat Thy Neighbor"

When dealing with emission regions closer than an arcsec to each other, another pernicious effect of pileup comes from the detection algorithm. Whenever a candidate event is found, any other event within its 3 × 3 pixel grid (for FAINT MODE) is considered to be a part of that event. Of the two (or more), the event with the most energy "wins" and its position determines the reported location, and its energy is found from the sum of the charges within the 3 × 3 grid. HST-1 and the nucleus are separated by 0.″86 or 1.75 pixels. Thus, in the normal course of events, there will be occasional conflicts of this sort involving a nuclear count arriving within the same frame time as one from HST-1. As the intensity of HST-1 rises, this will happen more often, and many times the nucleus will "win" because it has a harder spectrum than does HST-1. However, when pileup gets stronger, HST-1 will "win" most of the time since almost all events in a frame time will consist of at least two photons, boosting the recorded charge so as to exceed the single photon from the nucleus. We are unaware of any quantitative estimates of this effect, but suspect it is not causing any serious problems for our analyses when HST-1 is <4 keV s^{-1}.

A.3. Second-Order Effects of Pileup

When there is negligible pileup, the mutual overlap of the core and HST-1 PSFs is $\approx$5% $\pm$ 2% for the rectangular regions used for photometry (Figure 1). However, when pileup is significant, there are second-order effects which seriously distort the PSF. Although we avoid some of these by summing energy instead of just counts, there are others which cannot be accommodated: e.g., the release of trapped charge during readout. Since the most obvious of these produces a secondary response displaced a few pixels from the PSF in the direction away from the readout buffer, the primary effect on adjacent jet features changes with the roll angle. Given the celestial position of M87, the roll angle is such that there are long periods of relatively constant roll angles at the beginning and end of the M87 viewing season (November to August) and a rather rapid change by close to 180° centered around a date late in March. Since the P.A. of the readout streak is similar to that of the jet at the beginning and end of the season, the primary second-order effect produces contamination of jet features adjacent to HST-1 in the sense that prior to March the nucleus is badly affected whereas after the end of March it is knot D which suffers. This effect is evident in Figure 9.

The fact that this sort of second-order effect of pileup has not been calibrated (nor may be susceptible to calibration) means that changes in the measured intensity of the nucleus (and knot D) may not be intrinsic during the time that HST-1 was bright. For that reason, we have restricted usage of the core data to times when HST-1 was not too intense.

APPENDIX B

X-RAY INTENSITIES FOR THE NUCLEUS AND HST-1

In Paper III, we gave our measured intensities for HST-1 through 2005. Here, we repeat these and also provide uncertainties and the values for the nucleus (already with 5% of HST-1

Table B1
Chandra Dates and X-ray Intensities of the Nucleus and HST-1

Epoch	Observational Parameters		Live Time	Nucleus		HST-1	
Label	Date	ObsID	(s)	K[a] (keV s^{-1})	σ[b] (keV s^{-1})	K[a] (keV s^{-1})	σ[b] (keV s^{-1})
A[c]	2000 Jul 30	1808	12845	0.300	0.005	0.247	0.005
B	2002 Jan 16	3085	4889	0.644	0.014	0.734	0.013
C	2002 Feb 12	3084	4655	0.575	0.013	0.588	0.012
D	2002 Mar 30	3086	5089	0.536	0.013	0.576	0.012
E	2002 Jun 8	3087	4973	0.443	0.012	0.798	0.014
F	2002 Jul 24	3088	4708	0.494	0.013	1.096	0.017
G	2002 Nov 17	3975	5287	0.649	0.014	0.799	0.013
H	2002 Dec 29	3976	4792	0.652	0.014	0.653	0.013
I	2003 Feb 4	3977	5276	0.598	0.013	0.645	0.012
J	2003 Mar 9	3978	4852	0.777	0.016	0.872	0.015
K	2003 Apr 14	3979	4492	0.583	0.014	1.071	0.017
L	2003 May 18	3980	4788	0.378	0.011	1.022	0.016
M	2003 Jul 3	3981	4677	0.372	0.011	0.859	0.015
N	2003 Aug 8	3982	4841	0.304	0.010	1.214	0.018
O	2003 Nov 11	4917	5028	0.723	0.016	2.192	0.026
P	2003 Dec 29	4918	4677	0.384	0.012	2.041	0.026
Q	2004 Feb 12	4919	4703	0.515	0.016	4.079	0.04
R[d]	2004 Mar 29	4920	5235	...	...	...	...
S	2004 May 13	4921	5251	0.396	0.013	5.358	0.05
T	2004 Jun 23	4922	4543	0.228	0.013	5.323	0.05
U	2004 Aug 5	4923	4633	0.264	0.014	5.636	0.055
V	2004 Nov 26	5737	4237	0.740	0.022	7.494	0.07
W	2005 Jan 24	5738	4666	0.416	0.023	8.316	0.08
X	2005 Feb 14	5739	5154	0.439	0.024	8.785	0.08
Ya	2005 Apr 22	5740	4699	0.254	0.019	12.417	0.11
Yb	2005 Apr 28	5744	4699	0.505	0.022	12.167	0.11
Yc	2005 May 4	5745	4705	0.435	0.021	11.798	0.108
Yd	2005 May 13	5746	5142	0.557	0.022	11.555	0.10
Ye	2005 May 22	5747	4701	0.597	0.023	11.243	0.10
Yf	2005 May 30	5748	4699	0.268	0.018	10.665	0.10
Yg	2005 Jun 3	5741	4698	0.357	0.019	10.432	0.095
Yh	2005 Jun 21	5742	4703	0.252	0.018	10.270	0.094
Yi	2005 Aug 6	5743	4672	0.165	0.013	7.098	0.067
Yj	2005 Nov 29	6299	4655	0.514	0.016	4.032	0.042
Yk	2006 Jan 4	6300	4660	0.612	0.017	3.833	0.040
Yl	2006 Feb 19	6301	4337	0.861	0.020	3.535	0.040
Ym	2006 Mar 30	6302	4701	0.407	0.014	3.786	0.040
Yn	2006 May 21	6303	4699	0.377	0.013	3.161	0.035
Yo	2006 Jun 19	6304	4677	1.117	0.021	2.557	0.031
Yp	2006 Aug 2	6305	4653	0.802	0.018	2.246	0.028
Yq	2006 Nov 13	7348	4543	0.682	0.018	4.042	0.04
Yr	2007 Jan 4	7349	4685	0.703	0.018	3.642	0.039
Ys	2007 Feb 13	7350	4662	0.823	0.019	3.516	0.039
Yt	2007 Feb 15	8510	4701	0.641	0.017	3.428	0.038
Yu	2007 Feb 18	8511	4703	0.561	0.016	3.515	0.038
Yv	2007 Feb 21	8512	4703	0.694	0.017	3.479	0.038
Yw	2007 Feb 24	8513	4700	0.717	0.018	3.472	0.038
Yx	2007 Mar 12	8514	4471	0.722	0.018	3.443	0.039
Yy	2007 Mar 14	8515	4696	0.651	0.017	3.533	0.038
Yz	2007 Mar 19	8516	4679	0.716	0.018	3.599	0.039
Za	2007 Mar 22	8517	4674	0.775	0.019	3.571	0.039
Zb	2007 Mar 24	7351	4683	0.728	0.018	3.396	0.039
Zc	2007 May 15	7352	4588	0.432	0.014	2.968	0.034
Zd	2007 Jun 25	7353	4543	0.372	0.014	3.445	0.038
Ze	2007 Jul 31	7354	4707	0.236	0.011	3.383	0.037
Zf	2007 Nov 25	8575	4679	0.610	0.015	1.376	0.020
Zg	2008 Jan 5	8576	4692	0.628	0.015	1.230	0.019
Zh	2008 Feb 16	8577	4659	1.480	0.024	1.305	0.020

Table B1
(Continued)

Epoch	Observational Parameters		Live Time	Nucleus		HST-1	
Label	Date	ObsID	(s)	K^a (keV s^{-1})	σ^b (keV s^{-1})	K^a (keV s^{-1})	σ^b (keV s^{-1})
Zi	2008 Apr 1	8578	4706	0.743	0.017	1.493	0.021
Zj	2008 May 15	8579	4706	0.565	0.014	1.398	0.021
Zk	2008 Jun 24	8580	4705	0.950	0.019	1.293	0.020
Zl	2008 Aug 7	8581	4657	0.431	0.012	0.947	0.016

Notes.
[a] The values of K are "detector-based" observed intensities. They come from summing the energies of all events (from the "evt1" file) within a rectangle of length 5 pixels transverse to the jet and 2.5 pixels along the jet (Figure 1). No background subtraction was employed: when HST-1 is weak, the background (in counts) is of order 1%; for the highest intensity, the background is less than 0.3%. There is no correction for the buildup of ACIS contamination.
[b] Uncertainties are based on the raw counts: $\sqrt{N}/N$, hence 1σ.
[c] Archival data from Wilson & Yang (2002).
[d] This observation was taken in continuous clocking mode, so there is no two-dimensional image available. All other observations had 1/8th subarray ACIS-S3 chip only, and 0.4 s frame time.

subtracted), both through the current season which ended in 2008 August. As described in Paper III, we can estimate the "fudge factor," a, in the effective area by measuring the flux from fluxmaps when pileup is not serious. However, we plan to deal with spectral properties of the various features in a future paper so prefer to publish here only our directly determined intensities.

REFERENCES

Acciari, V. A., et al. (VERITAS Collaboration) 2008, ApJ, 679, 397
Aharonian, F., et al. (HESS Collaboration) 2006, Science, 314, 1424
Albert, J., et al. (MAGIC Collaboration) 2008, ApJ, 685, L23
Bicknell, G. V., & Begelman, M. C. 1996, ApJ, 467, 597
Bridle, A. H., & Greisen, E. W. 1994, AIPS Memo 87 (Charlottesville, VA: NRAO)
Cheung, C. C., Harris, D. E., & Stawarz, Ł. 2007, ApJ, 663, L65 (Paper IV)
Davis, J. E. 2001, ApJ, 562, 575
Ergin, T. (for the VERITAS Collaboration) 2008, in Radio Galaxies in the *Chandra* Era, http://cxc.harvard.edu/radiogals08/pres/T_Ergin.pdf
Georganopoulos, M., Perlman, E. S., & Kazanas, D. 2005, ApJ, 634, L33
Harris, D. E., Biretta, J. A., Junor, W., Perlman, E. S., Sparks, W. B., & Wilson, A. S. 2003, ApJ, 586, L41 (Paper I)
Harris, D. E., Cheung, C. C., Biretta, J. A., Sparks, W., Junor, W., Perlman, E. S., & Wilson, A. S. 2006, ApJ, 640, 211 (Paper III)
Harris, D. E., Cheung, C. C., Stawarz, Ł., Biretta, J. A., Sparks, W., Perlman, E. S., & Wilson, A. S. 2008, in ASP Conf. Ser. 386, Extragalactic Jets: Theory and Observation from Radio to Gamma Ray, ed. T. A. Rector & D. S. DeYoung (San Francisco, CA: ASP), 80
Kardashev, N. A. 1962, SvA, 6, 317
Levinson, A. 2000, PRL, 85, 912
Marshall, H. L., et al. 2005, ApJS, 156, 13
Pacholczyk, A. 1970, Radio Astrophysics (San Francisco, CA: Freeman)
Perlman, E. S., Harris, D. E., Biretta, J. A., Sparks, W. B., & Macchetto, F. D. 2003, ApJ, 599, L65 (Paper II)
Shepherd, M. C., Pearson, T. J., & Taylor, G. B. 1994, BAAS, 26, 987
Tavecchio, F., & Ghisellini, G. 2008, MNRAS, 385, 98
Tonry, J. L. 1991, ApJ, 373, L1
Wilson, A. S., & Yang, Y. 2002, ApJ, 568, 133